Laser-Assisted Micro-Pulsejet Thruster

Hideyuki Horisawa and Sou Eto

Department of Aeronautics and Astronautics, Tokai University
Hiratsuka, Kanagawa, 259-1292, Japan

Abstract. A fundamental study of a laser-assisted micro-pulsejet thruster was conducted for a candidate of next-generation air-breathing micro-thruster systems. CFD analyses were conducted to evaluate internal phenomena, thrust performances, and influence of exhaust orifice for propellants of hydrogen-air mixture. Experimental investigations were also conducted to evaluate influence of exhaust orifices and the optimum configuration of the micro-combustion chamber. From the results, it was shown that the exhaust orifice was more effective for the improvement of thrust performance. Moreover, influence of combustor geometry on thrust performance for the improvement was confirmed. In our simulation and experimental results, the efficiency from ideal chemical energy, which is expected to be released from an ideal hydrogen-air mixture, into kinetic energy was a few percents. There are still some ways to recover this amount of loss with optimum combustor geometries and higher laser energies, and potential achieving much higher thrust performances.

Keywords: Laser ignition, Micro-pulsejet thruster, Laser-induced plasma, Laser-assisted combustion
PACS: 52.30.Cv, 52.35.Tc, 52.38.-r, 52.75.Di, 47.70.Pq

INTRODUCTION

Recent significant development of microelectromechanical systems (MEMS) and precision mechanical machining techniques along with evolution of high-functional materials has enabled various novel micro-electronic devices used in many fields. In aerospace engineering fields, for example, small-sized satellites such as micro- and nano-satellites, and unmanned micro aerial vehicles (MAVs) are under significant development in many countries. Some of the primary elements of these systems are fabricated with those techniques. Specific to controlling aerial vehicles in atmosphere, they are subjected to relatively large aerodynamic forces, and these forces can be used for position and attitude control mechanisms. Utilization of the aerodynamic forces can vary the type of the mechanisms or configurations of vehicles such as fixed-wings, rotating-wings, or beating-wings, aimed for various purposes.

Authors have been developing the micro air-breathing thrusters, which can be utilized either for primary propulsion engines or attitude control thrusters, or for both purposes. The main objective of this development is to achieve the microthrusters capable of both highspeed transportation and stable hovering. Various small-sized air-breathing propulsion systems such as turbojet and pulsejet engines have been developed for decades and some of them at present are commercially available mostly for hobby-airplane use. Among these systems, authors have been focusing on pulsejets. None of turbo-machinery elements are used in this type of engine, and the propulsion system can be very simple and lightweight. In addition, comparing to other air-breathing systems, its specific impulse and thrust efficiency are relatively high. Although these advantages, noise produced through the pulse operation is the primary issues.

To achieve the increased initial pressure and namely smaller diameter of the combustor, authors have been trying to use the blast waves induced with focused laser beams. Depending on laser energy, strength of the initial blast wave can be controlled. With this process, initial internal pressure inside the combustor can be abruptly increased [1].

Small-sized combustors are of our primary interest, since ratios of laser energies to heat release from combustion reaction of the combustor can be easily controlled. Therefore, augmented ignition techniques such as laser ignition can be utilized and effective. Along with the miniaturization, area-to-volume ratios of the combustors will increase. With the increased ratios, surface catalytic reactions can be utilized effectively for augmentation of ignition reactions. Moreover, since they are small, the repetitive pulse operation can be in high-repetition rate with proper air-intake mechanisms capable of high-repetition

CP1282, *New Trend in Applied Plasma Science and Technology – ISAPS '09*
edited by A. Kobayashi, T. Miyasaka, and J. Krasa

operation. In addition, total force acting on an inner surface of the combustor can be insignificant due to the small surface area. Therefore, strength of the combustor wall can be easily maintained.

In this study, an assessment of thruster performance was conducted by computational fluid dynamic simulations. Our concerns are to elucidate the effects of laser augmentation in the small combustor, combustor configuration and ignition points. Moreover, a fundamental experiment of a laser-augmented micro-pulsejet thruster was also conducted. Thrust performances were tested with a ballistic pendulum type thrust-stand for propellants of hydrogen-air mixtures with various equivalence ratios. Spark-ignition and laser-ignition were also compared to elucidate the optimum ignition schemes and conditions.

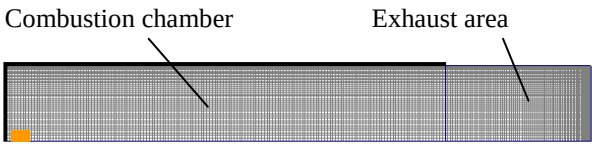

FIGURE 1. Calculation model.

TABLE 1. 16 elementary reactions with 10 species for hydrogen-air mixture.

1	$H_2 + O_2$	⇔	$OH + OH$
2	$H_2 + OH$	⇔	$H_2O + H$
3	$H + O_2$	⇔	$OH + O$
4	$O + H_2$	⇔	$OH + H$
5	$H + O_2 + N_2$	⇔	$HO_2 + N_2$
6	$OH + HO_2$	⇔	$H_2O + O_2$
7	$H + HO_2$	⇔	$OH + OH$
8	$O + HO_2$	⇔	$O_2 + OH$
9	$OH + OH$	⇔	$O + H_2O$
10	$H_2 + N_2$	⇔	$H + H + N_2$
11	$O_2 + N_2$	⇔	$O + O + N_2$
12	$H + OH + N_2$	⇔	$H_2O + N_2$
13	$O + N_2$	⇔	$NO + N$
14	$N + O_2$	⇔	$NO + O$
15	$OH + N$	⇔	$NO + H$
16	$H + HO_2$	⇔	$H_2 + O_2$

SIMULATION OF MICRO-PULSEJET THRUSTER

Model Assumption and Calculation Model

We conducted the numerical analysis to verify hydrodynamic and chemical-reaction effects on ignition and subsequent impulse generation phenomena with computational fluid dynamic (CFD) analyses. In the analyses a commercial CFD code, CFD2000 (Adaptive Research Inc.), was utilized. A numerical thruster model consists of a cylindrical combustion chamber (inner diameter of 10 mm x length of 30 mm) having an open orifice and another edge closed. In the analyses, a two-dimensional rectangular geometry is assumed, which consists of an upper half of the chamber from the centerline as shown in Figure 1. A lower side of this model is assumed as a reflective condition and an extra exhaust volume is added after the orifice exit. In the calculation, a time-dependent Navier-Stokes equation including finite rate chemistry of 16-step-elementary reactions of a hydrogen-air mixture is solved.

The sixteen pairs of elementary reactions for 10 species (H_2, O_2, O, H, N, OH, NO, H_2O, HO_2 and N_2) employed in this simulation are listed in Table 1.

As for an initial propellant filling of the combustor a hydrogen-air mixture with an ideal mixture of its equivalence ratio of unity was assumed at a pressure of 101.3 kPa and a temperature of 298.15K. To model a focused laser beam or laser induced plasma, several attempts have been conducted [2-8]. Since the laser pulse used is shorter than 10 nsec, its short-duration heating process can be regarded as if occurring under a constant volume condition. For this reason, a high-enthalpy laser-induced plasma kernel is assumed as a hot-gas spot with finite size to which it has developed from an initial micro-plasma nucleus [8]. Since it is confirmed from our experiment that an initial plasma, or hot spot, is as big as 1 ~ 2 mm in diameter at initial 100 nsec, initial size of the spherical hot spot used in this simulation is assumed to be 1 ~ 2 mm in diameter depending on laser pulse energies. Initial pressure and temperature of the hot spot, or laser-induced plasma, were assumed as 1.0 MPa and 3,000 K, respectively. Similar to our experimental conditions, a focal point of the laser beam, or location of the initial plasma, was placed nearby the closed edge on the centerline.

In our simulation, first of all, an assessment of effects of the orifice diameter on impulse-bits was conducted. The impulse-bit was calculated by integrating temporal changes of local pressures on inner walls of the combustor, as follows,

$$I_{bit} = \int_0^t \int_A (P_h - P_a) \cdot dA dt, \quad (1)$$

where p_h: local wall pressure, p_a: ambient (atmospheric) pressure, dA: elemental area at wall, A: total wall area in the simulation domain, t: typical pressure wave duration (1 msec). Secondly, influences of the initial laser-focal points, or laser-induced plasma positions, were investigated. In this simulation, several positions from 0 mm to 30 mm away from the initial focal point at the closed-side of edge were tested as illustrated in Fig.1. Impulse-bits for each case was estimated and then compared.

Result of Calculation

Behaviors of pressure wave propagation are shown in Figure 2. It can be seen that the mixture is ignited with a laser-induced plasma and a pressure wave is running toward the orifice. The pressure wave is arriving at the orifice in about 36 μsec after ignition. According to the duration and the distance between the orifice and combustor edge, an average velocity of the pressure-wave propagation is about 833 m/sec. This velocity is faster than the acoustic velocity for the initial flow field.

Temporal variations of internal pressure on centerline at the closed-edge are shown in Figure 3, in which influence of the orifice sizes, between 4 mm and 10 mm in diameters, is compared. With the 10 mm orifice, or without orifice, the internal pressure converges down to ambient pressure at 0.4 msec. Whereas with 4 mm orifice, the advantage in high-pressure becomes significant from 0.1 msec, and it can be maintained for a longer duration which is converging down to ambient pressure at 0.8 msec. The effect of the orifice is remarkable keeping internal pressure higher for longer duration time.

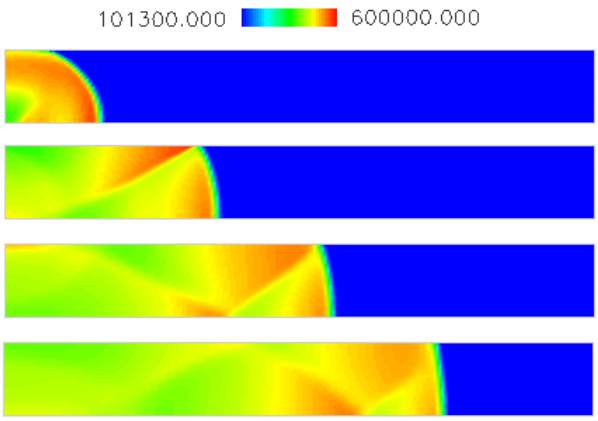

FIGURE 2. Propagation of pressure wave.

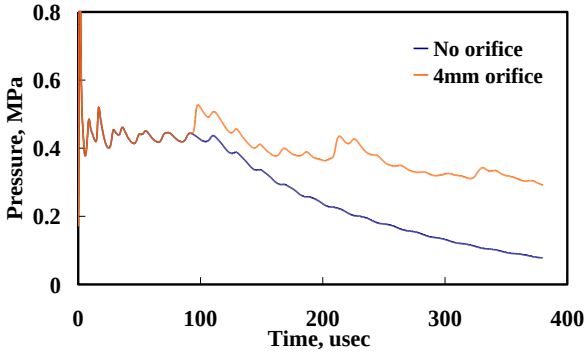

FIGURE 3. Temporal variations of pressure at closed edge center.

TABLE 2. Impulse bit (no orifice & orifice).

	Impulse bit, Nsec/m^2
No orifice	81.6
4mm orifice	150

TABLE 3. Impulse bit (Ignition point).

distance, mm	Impulse bit, Nsec/m^2
0	79.5
10	83.1
20	83.2
30	83.8

The values of impulse-bits calculated from Eq. (1) for above different orifice conditions are listed in Table 2. From the results, the impulse-bit with 4 mm orifice is augmented about 2 times greater than that without orifice. This is due to the higher internal pressure maintained for longer duration.

Results for influences of the laser-focal point on impulse-bit generation are listed in Table 3. Although little difference can be seen among these results, within 1 to 2 %, larger distance of the ignition point away form the closed edge showed slightly greater values of impulse-bits.

EXPERIMENTAL

Impulse-bit Measurement

A photo of a thruster is shown in Figure 4. The thruster consists of a cylindrical combustion chamber (inner diameter of 10 mm x length of 30 mm) and an

initiator part (inner diameter of 10 mm x length of 5 mm) both made of aluminum.

Schematics of experimental setups showing different ignition methods, i.e. a spark ignition and laser ignition, are illustrated in Figures 5 (a) and (b), respectively. In this experiment, a hydrogen-air mixture is used for the propellant. After determining mass flows of hydrogen and air, or an equivalence ratio with solenoid valves, the mixture was introduced into the combustion chamber. In the spark ignition, an electric circuit consisting of a DC charger, a capacitor of 1 μF, and discharge igniter was developed and tested. The capacitor can be charged up to 590 V. As for a miniaturized ignition plug, an in-house plug consisting of a tungsten-rod cathode of 3 mm in diameter and an annular stainless anode of 5 mm in outer-diameter was used. Changing charge voltages V to the capacitor C, ignition energy E ($E = CV^2/2$) can be controlled. On the other hand, in laser ignition, a laser pulse from an Nd:YAG laser (QUANTEL LPY 150-10/20, wavelength: 1064 nm, maximum pulse energy: 335 mJ/pulse, pulse width: 5 nsec) was irradiated and focused with a focusing lens of f = 150 mm into an initiator part of a cylindrical combustion chamber filled with a hydrogen-air mixture of a controlled equivalence ratio. Then a chemical detonation is initiated with a laser-induced plasma, and an impulse is generated on the nozzle.

To elucidate influences of ignition method and energy, thrust performance tests were conducted. To measure a single impulse of μNsec-class, a thrust stand was developed and utilized. The thrust stand, shown in Figure 6, consists of a ballistic pendulum. As for its pivot, a knife edge was used. The pendulum is made of an aluminum member of 456 mm in length and 25 mm x 25 mm in cross section. A counter weight was placed in another side of the pendulum to make the pivot as a center of impact. An eddy-current type displacement sensor was used to measure the displacement of the pendulum. A schematic of an experimental setup for impulse-bit measurement is shown in Figure 7. The pendulum receives a reaction force from the thruster and then a displacement or impulse is to be measured. The displacement induced at each impulse generation was calibrated with an impact of a steel ball at each shot.

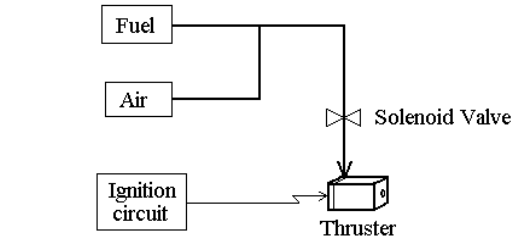

(a) Spark ignition

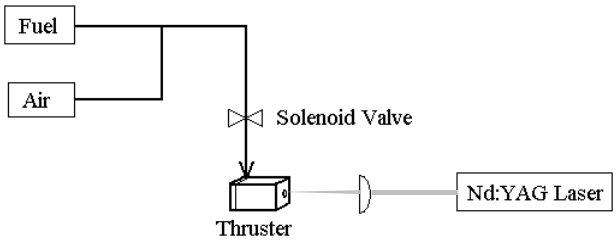

(b) Spark ignition

FIGURE 5. Schematics of ignition system.

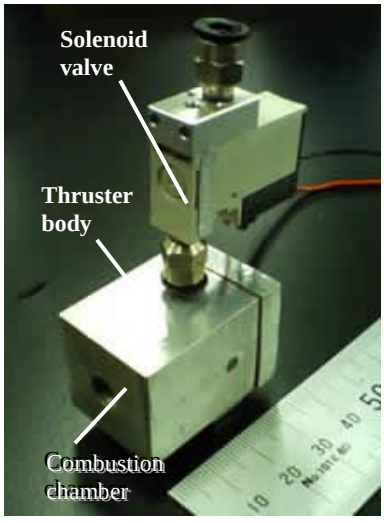

FIGURE 4. Photo of micro thruster.

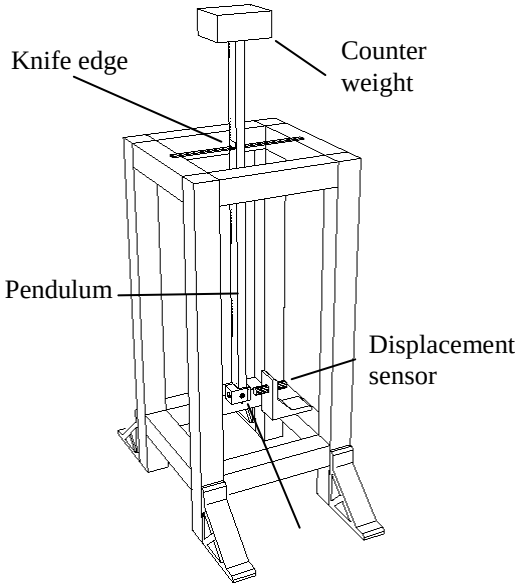

FIGURE 6. Schematic of impulse measurement system.

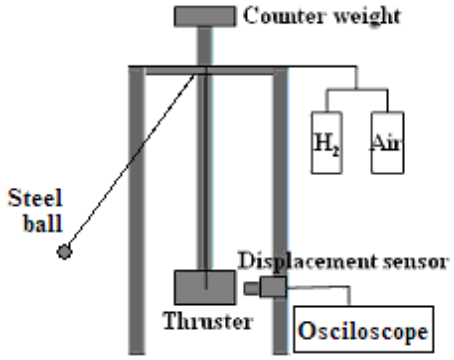

FIGURE 7. Schematic of calibration setup.

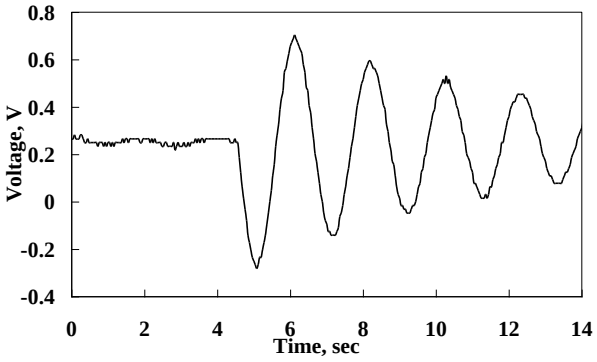

FIGURE 8. Typical output signal of displacement sensor.

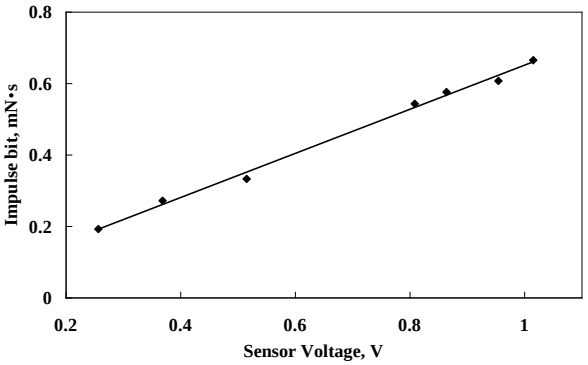

FIGURE 9. The result of calibration experiment.

Calibration of Thrust Stand

A schematic of an experimental setup for impulse-bit calibration is also illustrated in Fig.7. The pendulum receives a reaction force from the thruster and then a displacement or impulse is to be measured. The displacement induced at each impulse generation was calibrated with an inelastic impact of an aluminum ball suspended with a string released from an arbitrary height at each measurement, giving an arbitrary impulse to the thruster. A typical output signal of the displacement sensor is shown in Figure 8.

The relation of the amplitude of the first peak of the signal from the displacement sensor versus arbitrary impulse is plotted in Figure 9. The impulse was calculated from the height and mass of the impacting ball. As shown in this figure, linear relations between impulse and sensor amplitude can be obtained. From this linear relation, measured values of impulse-bits were estimated.

RESULTS AND DISCUSSION

Comparison of Thrust Performances between Spark Ignition and Laser Ignition

Comparison of thrust performances between conventional spark ignition and laser ignition is shown in Figure 10, in which effects of equivalence ratio of hydrogen/air mixtures on impulse-bit are plotted. From the figure, it can be seen that the impulse-bit rapidly increases with equivalence ratios of ϕ = 0.8 to 1.2 and then gradually decreases, showing peak values at ϕ = 1.2 for each case. The peak values for spark ignition and laser ignition are 0.14 mNsec and 0.23 mNsec, respectively.

From these results, it is shown that higher impulse-bits can be obtained with laser ignition. Since a peak power of the laser pulse in this experiment is high enough to induce an initial blast wave at the focal point initiating a strong reacting wave, a higher impulse can be generated more effectively than through conventional spark ignitions.

Effect of Orifice Size on Thrust Performance

Comparison of thrust performances among different orifice sizes, i.e., 4mm, 6 mm and 10 mm, is shown in Figure 11, in which effects of equivalence ratio of hydrogen/air mixtures on impulse-bit are also plotted. From the figure, it can be seen that the impulse-bit rapidly increases with equivalence ratios of ϕ = 0.8 to 1.2 and then gradually decreases, showing peak values at ϕ = 1.2 for each case. The peak values for 10mm-orifice, 6mm-orifice and 4mm-orifice are 0.79 mNsec, 0.92 mNsec and 1.03 mNsec, respectively. From the result, it is shown that higher impulse bit can be obtained with smaller orifices. It is also shown that the effect of the orifice is more significant when the equivalence ratio exceeds unity.

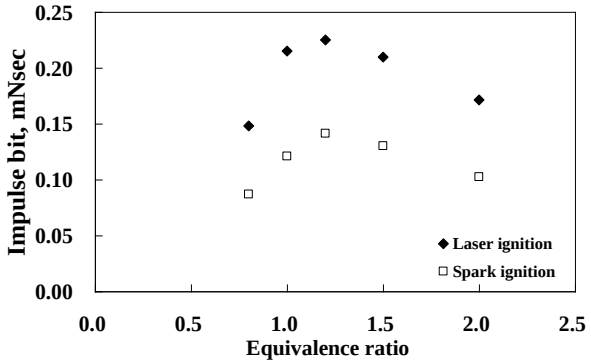

FIGURE 10. Impulse-bit (ignition energy 175mJ).

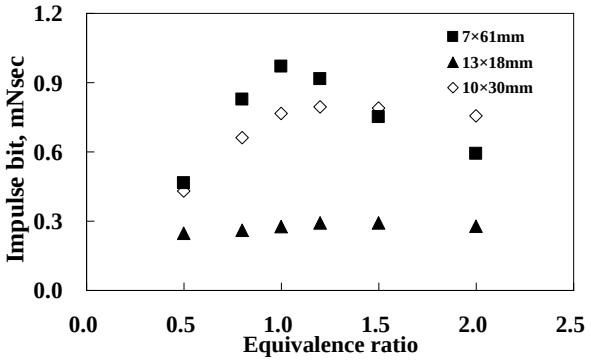

FIGURE 12. Impulse-bit for different geometries.

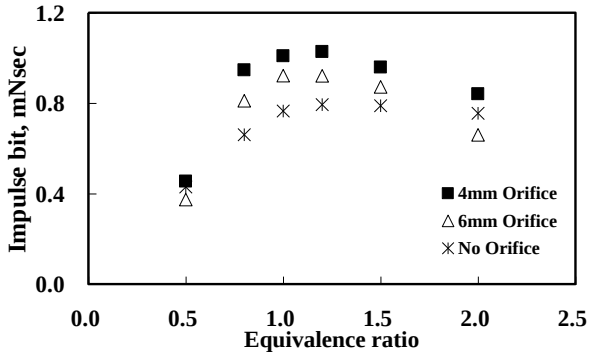

FIGURE 11. Effect of orifice size on impulse-bit.

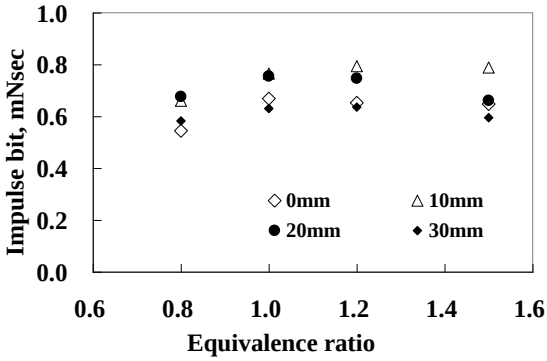

FIGURE 13. Impulse-bit for various ignition points.

Influence of Combustor Geometry on Thrust Performance

Comparison of thrust performances between two different combustors is shown in Figure 12, in which effects of equivalence ratio of hydrogen/air mixtures on impulse-bit are also plotted. The volume of each combustor is identical, about 3.5 cc, while the inner diameter of one of them is 10 mm and another of 7 mm. The peak value of impulse-bit for 7mm-combustor is 0.97 mNsec at ϕ =1.0. From the result, it is shown that significantly higher impulse bit can be obtained with the narrower-shape combustor.

Comparison of thrust performances among different ignition points is shown in Figure 13. In each case, the peak values appear at equivalence ratio of unity. Also, it can be seen that impulse-bits for ignition points of 10 mm and 20 mm away from the closed-side of combustor are about 20 % higher than those of 0 mm and 30 mm ignition in whole equivalence ratio region. Moreover, the 10 mm case seems less sensitive to equivalence ratio.

From the result, it is confirmed that there is an optimum laser-focal position for ignition and impulse generation. The local equivalence ratio near the orifice can be low through the diffusion to external atmosphere,. Then the local flame speed, when ignited at near-orifice position, may be slow causing a weak local pressure wave.

From these results, it is shown that even a small thruster can generate relatively high impulses when some optimum conditions are achieved. In our simulation and experimental results, the efficiency from ideal chemical energy, which is expected to be released from an ideal hydrogen-air mixture, into kinetic energy is a few percents. There are still ways to recover this amount of loss with optimum combustor geometries and higher laser energies, and potential achieving much higher thrust performances.

CONCLUSIONS

A fundamental study of a laser-assisted micro-pulsejet thruster was conducted for a candidate of

next-generation air-breathing micro-thruster systems. CFD analyses were conducted to evaluate internal phenomena and thrust performances for propellants of hydrogen-air mixture, including effectiveness of an exhaust orifice. Experimental investigations were also conducted to evaluate the effectiveness of the orifice and optimum geometries of the micro combustor. Following conclusions were obtained.

(1) An increase in laser energy and reduction of orifice diameter were more effective for the improvement of thrust-performance due to the generation of higher internal pressure with longer duration.
(2) Narrower configuration of the combustor also proved effective.
(3) In both simulation and experiment, the conversion efficiency from ideal chemical energy, expected to be released from an ideal hydrogen-air mixture, into kinetic energy was a few percents.

REFERENCES

1. A. N. Pirri, M. J. Monsler, and P. E. Nebolsine, "Propulsion by Absorption of Laser Radiation", *AIAA. J*, **12**, 9 (1974).
2. K. Komurasaki, , Proc. 46th Symposium on Space Science and Technology, 2002, pp.1439-1444.
3. H. Katsurayama and Y. Arakawa, *J. Japan Soc. Aeronautical and Space Sci.*, **53**, 47-50 (2005).
4. H. Katsurayama and Y. Arakawa, *Applied Plasma Science*, **12**, 17-22 (2004).
5. T. Miyasaka and T. Fujiwara, *Beamed Energy Propulsion*, AIP Conference Proceedings 702, 2004, pp.80-91.
6. H. Shiraishi and T. Fujiwara, *J. Japan Soc. Aeronautical and Space Sci.*, **46**, 607-613 (1998).
7. T. Fukui and T. Fujiwara, *J. Japan Soc. Aeronautical and Space Sci.*, **43**, 619-625 (1995).
8. D. V. Ritzel and K. Matthews, Proc. of 21st Internal Symposium on Shock Waves, 1997, pp.97-102.